



Contents lists available at ScienceDirect

Spectrochimica Acta Part A: Molecular and Biomolecular Spectroscopy

journal homepage: www.elsevier.com/locate/saa

Locations of radical species in black pepper seeds investigated by CW EPR and 9 GHz EPR imaging

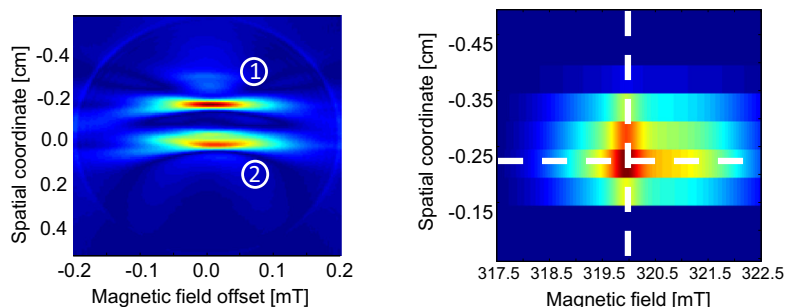
Kouichi Nakagawa^{a,*}, Boris Epel^b^aDepartment of Radiological Life Sciences, Graduate School of Health Sciences, Hirosaki University, 66-1 Hon-cho, Hirosaki 036-8564, Japan^bDepartment of Radiation and Cellular Oncology, The University of Chicago, MC1105, 5841 S. Maryland Ave, Chicago, IL 60637-1463, USA

HIGHLIGHTS

- Locations of radical species in black pepper seeds were investigated by continuous wave (CW) EPR and 9 GHz EPR imaging.
- Lithium phthalocyanine (LiPC) phantom was used to examine 9 GHz EPR imaging capabilities.
- Radical species were mostly located at the seed surface.
- CW EPR and EPR imaging were useful for determination of the spatial distribution of paramagnetic species in various seeds.

GRAPHICAL ABSTRACT

Spectral–spatial images of lithium phthalocyanine (LiPC) phantom (left-hand) and a pepper seed (right-hand).



ARTICLE INFO

Article history:

Received 13 January 2014

Received in revised form 11 April 2014

Accepted 22 April 2014

Available online 30 April 2014

Keywords:

EPR
Imaging
Free radical
LiPC
Pepper
ESR

ABSTRACT

In this study, noninvasive 9 GHz electron paramagnetic resonance (EPR)-imaging and continuous wave (CW) EPR were used to investigate the locations of paramagnetic species in black pepper seeds without further irradiation. First, lithium phthalocyanine (LiPC) phantom was used to examine 9 GHz EPR imaging capabilities. The 9 GHz EPR-imager easily resolved the LiPC samples at a distance of ~ 2 mm. Then, commercially available black pepper seeds were measured. We observed signatures from three different radical species, which were assigned to stable organic radicals, Fe^{3+} , and Mn^{2+} complexes. In addition, no EPR spectral change in the seed was observed after it was submerged in distilled H_2O for 1 h. The EPR and spectral–spatial EPR imaging results suggested that the three paramagnetic species were mostly located at the seed surface. Fewer radicals were found inside the seed. We demonstrated that the CW EPR and 9 GHz EPR imaging were useful for the determination of the spatial distribution of paramagnetic species in various seeds.

© 2014 Elsevier B.V. All rights reserved.

Introduction

Electron paramagnetic resonance (EPR) or electron spin resonance (ESR) spectroscopy utilizes the electron-spin resonance phenomenon and measures the resonant microwave power absorption

* Corresponding author. Tel./fax: +81 172 39 5921.

E-mail address: nakagawa@cc.hirosaki-u.ac.jp (K. Nakagawa).

spectra of unpaired electrons subjected to a constant magnetic field in an atom, a molecule, or a compound. EPR is capable of noninvasively measuring samples. The majority of the EPR research in food has concentrated on free radicals in irradiated and/or powdered foodstuff [1–4] rather than endogenous species. EPR imaging is a powerful noninvasive technique for measuring the spatial distribution of paramagnetic species [5–7]. Two-dimensional (2D) spectral–spatial imaging provides information on both the distribution and

line-width of paramagnetic species. Thus, the noninvasive EPR imaging and continuous wave (CW) EPR can provide quantitative information about detailed paramagnetic species.

In the areas of food science and research, identification of localized paramagnetic species in foodstuffs is an important subject. Knowledge of the location (region) of paramagnetic (or free radicals induced) species can guide the further research on the biochemistry or chemistry of the species. The EPR imaging of the radical species may give information about the location of the species. The information may provide important insights for improving of the regarding food processing, conservation strategy, and shelf life.

Current applications of *in vivo* EPR imaging mostly concentrate on small animal imaging at frequencies below 1 GHz [8,9]. These EPR frequencies are dictated by the reduction in the microwave irradiation penetration depth in sample tissues at higher frequencies. The imaging of small specimens does not have to be restricted to low frequencies. Generally, the 9 GHz EPR imager is 1–200 times more sensitive than the 1 GHz EPR imager [10]. The sensitivity of the 9 GHz EPR allows it to detect paramagnetic species in materials, such as ascorbic acid in blood [11] and carbon-centered organic radicals in food [1].

In the present study, we investigated the location of paramagnetic species in black pepper seeds without further irradiation and chemical treatment using the CW 9 GHz EPR and EPR imaging. We also studied LiPC crystals that were spaced 2 mm apart. In addition, we analyzed the distribution of paramagnetic species in pepper seeds. We have also discussed the application of the EPR imaging and CW EPR techniques for food monitoring.

Materials and methods

Samples

Commercially bottled black pepper seeds were purchased from a local super market about five years ago. The seeds were used as purchased. One seed (~0.02 g) was inserted into an EPR tube (o.d. 5.0 mm, i.d. 4.0 mm, Wilmad-LabGlass, USA) for measurements.

Lithium phthalocyanine (LiPC) crystals used in our study were provided by Prof. H.M. Swartz (Dartmouth Medical College) and used as given [12]. LiPC is useful for EPR oximetry due to its sensitivity to oxygen. In our measurements, the LiPC crystals were attached to a plastic plate (~3 mm wide) using commercially available synthetic rubber-type glue. The phantom was composed of 2 LiPC point samples in the layout shown in Fig. 1. The first and second LiPC crystals were 2 mm apart. For the measurements, the LiPC phantom was inserted into an EPR tube.

EPR measurements

For 9 GHz EPR imaging, one set of gradient coils with an anti-Helmholtz coil configuration was used. To avoid overheating, the gradient coils were cooled using water. A Techron 7570 power supply (Indiana, USA) was used. The maximum available field gradient along the z-axis was approximately 9 mT/cm. All CW EPR spectra were obtained with a single scan.

Typical EPR imaging settings were as follows: microwave power, 5 mW; time constant, 1 s; sweep time, 2 min; magnetic field modulation, 0.3 mT; and sweep width, 15 mT. All measurements were performed at ambient temperature.

Imaging data processing

The first-derivative EPR spectra were numerically integrated to obtain the corresponding absorption spectra. For 2D spectral-spatial EPR imaging, we used 16 projections obtained with gradients

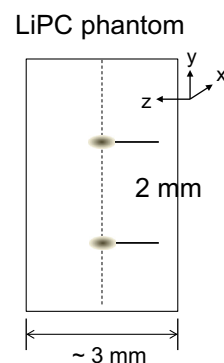


Fig. 1. Schematic of the used LiPC phantom. The coordination is indicated.

(G_i) from 0 to ~6.5 mT/cm. The projections were centered on the crossover magnetic field truncated to

$$\text{SWEEP}_i = \sqrt{2} dB / \cos(\theta_i), \quad (1)$$

where $\theta = \tan^{-1}(G_i \times dL/dB)$, scaled by $\cos(\theta_i)$ and resampled to 100 points [13]. The magnetic field support (dB) was 2 mT, and the spatial support of the image was 1 cm. Then, the data were back-projected to obtain a 2D spectral-spatial image using a filtered back-projection algorithm. The data were processed in the MathWorks MATLAB™ environment, and the “iradon” function was used for back-projection. The details of EPR and data processing are also described previously [5].

Results and discussion

EPR imaging of LiPC (phantom)

For the initial test, the LiPC phantom was imaged. Fig. 1 shows a schematic of the LiPC phantom. The glued LiPC crystals were ~2 mm apart. Fig. 2 shows the EPR spectra at different field gradient strengths. The top spectrum in Fig. 2 shows the phantom measured without the field gradient. The EPR spectrum has a strong single EPR line. The bottom spectrum shows the phantom measured with a ~6.5 mT/cm field-gradient. The spectrum in Fig. 2 clearly shows a minimum of two separate peaks. Thus, the EPR imager could resolve paramagnetic species separated by 2 mm.

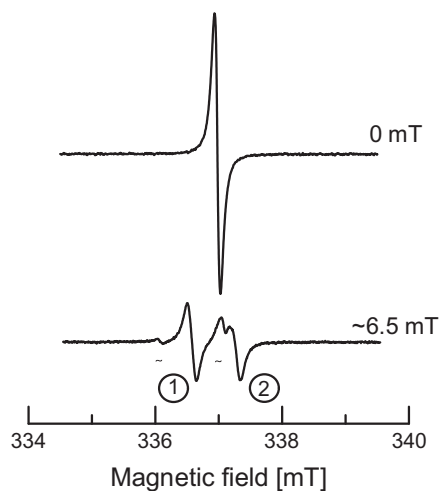


Fig. 2. The EPR spectra observed by the EPR imager with 0 mT/cm (top spectrum) and 6.5 mT/cm (middle spectrum). The filled triangles indicate a small amount of LiPC away from the main points due to the strong static repulsion of the crystals.

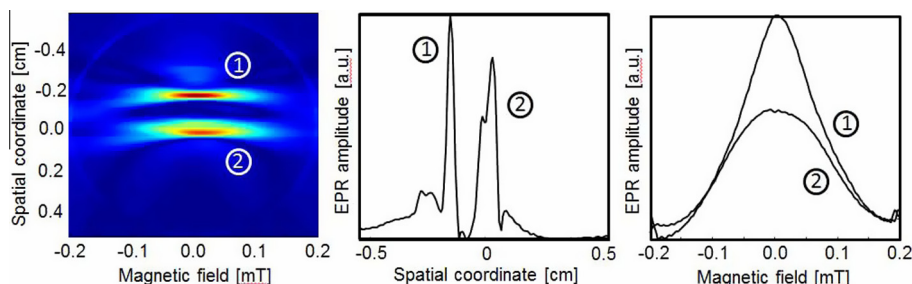


Fig. 3. 2D (spectral-spatial) imaging of the LiPC phantom. Two compositional diagrams of 2D imaging in Fig. 2 are presented. The middle and right-hand panels indicate the absorption mode of the EPR spectra (peaks ① and ②) in the spatial and magnetic field coordination, respectively.

It was noted that the small additional peaks indicated by the filled triangles were because of small LiPC crystals beside the two main crystals. As mentioned in the method section, the LiPC crystals repelled each other because of the strong static electrical charges.

The left panel of Fig. 3 shows a 2D (spectral-spatial) image of the LiPC phantoms. The two areas indicated by ① and ② correspond to the two peaks in Fig. 2. The middle panel of Fig. 3 shows the spatial dimension at the maximum of EPR lines. Two strong peaks were obtained after data processing. The right panel of Fig. 3 shows the EPR signal as a function of the magnetic field. Two signals of the EPR spectrum at spatial positions ① and ② are displayed. Thus, the 9 GHz EPR imaging of the phantom proves the existence of two paramagnetic species in ~ 2 mm apart.

EPR imaging of pepper (seeds)

Fig. 4 shows a picture of a pepper seed. The seed has a folded uneven surface. We measured the whole pepper seed that was

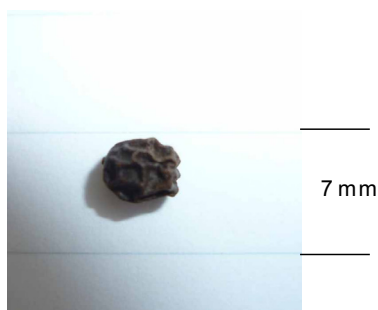


Fig. 4. Picture of a black pepper seed. The scale is indicated.

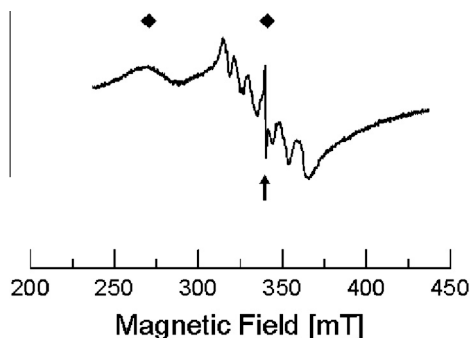


Fig. 5. Wide-range scan of the EPR spectrum for a black pepper seed. The spectrum was taken with a 200 mT sweep width. There are three species. The first is Fe^{2+} related signals (two filled diamonds) indicating $g = 2.50$ and $g = 1.98$, respectively. The second is Mn^{2+} related signals (6 lines). The third (arrow) is a relatively sharp signal related to an organic radical.

inserted into an EPR tube. Fig. 5 shows the EPR spectrum of a whole pepper seed. The spectrum was taken with a 200 mT scan-width. The spectral lines are attributed to three distinguishable paramagnetic species. One has a relatively sharp feature, which is indicated by the arrow. The feature could be the stable organic radicals – such as carbon-centered radicals [1]. The line-width (ΔH_{pp}) is ~ 0.7 mT.

The second one was a characteristic Mn^{2+} related sextet ($M_I = 5/2$, natural abundance is 100%) [14]. The third one could be Fe^{3+} , which is a broad feature indicated by filled diamonds. The two filled diamonds indicate field positions corresponding to $g = 2.50$ and $g = 1.98$. The g -values of the spectrum shown in Fig. 5 were calculated using the following:

$$h\nu = g\beta H, \quad (2)$$

where ν is the microwave frequency, g is the g -value, β is Bohr magneton, and H is the applied magnetic field. Based on the g -values of the peaks, paramagnetic species can be iron complexes [15]. Noted that the magnetic field of the EPR spectrometer was controlled by the current in order to perform EPR imaging (field gradient). The

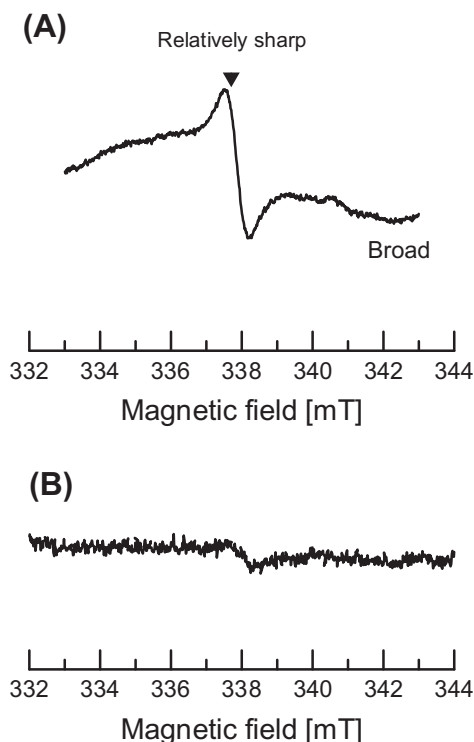


Fig. 6. The EPR spectra of the whole black pepper seed. Top spectrum is a whole black pepper seed. The bottom spectrum is the inner portion of the pepper seed.

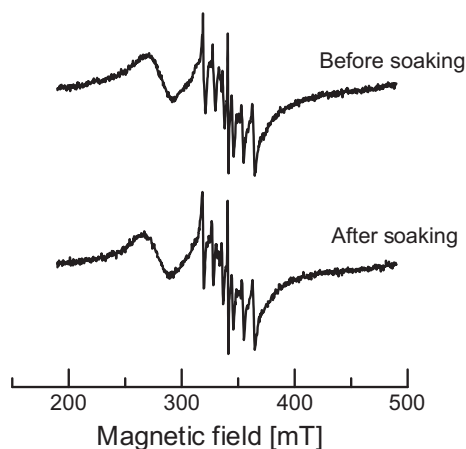


Fig. 7. The EPR spectra taken before soaking (A) and after soaking (B). The sample was soaked in distilled water (1 mL) for 1 h and dried for 5 h at ambient temperature.

g -values may not be very accurate because the magnetic field is not monitored by the NMR probe.

The EPR spectra composed of the sextet were attributed to Mn^{2+} peaks. The apparent changes in hyperfine couplings from low to high fields were larger at a high field due to overlapping with other features. Previously, a similar EPR spectrum was observed in powder black pepper [1]. The relatively sharp single-peak at $g = 1.99$ can be because of stable organic carbon-centered radicals or transition metal ions [15].

To verify the localization of radical species in the pepper seed, we broke it into two parts that included outer and inner portions of the seed. The EPR spectrum of outer part with a 30 mT scan is shown in Fig. 6 (top spectrum). The peak-to-peak width (ΔH_{pp}) of the relatively sharp feature was ~ 0.68 mT. The EPR spectrum of the inner portion of the pepper is shown in Fig. 6 (bottom spectrum). After removing surface area of the pepper, the remaining part was inserted into an EPR tube. A relatively sharp feature was observed.

In addition, we examined the effect of humidity on paramagnetic species in the pepper seed. The sample was soaked in distilled water (1 mL) for 1 h and dried for 5 h at ambient temperature. It was noted that the solution became brown in color after submerging the seed. EPR measurements were then performed on the seed. The EPR intensities of the soaked seeds were the same as those that were not soaked, as shown in Fig. 7. No difference in the spectra of the two samples were detected.

We attempted to reveal the distribution of paramagnetic species in the seed using a 9 GHz EPR imager. The 2D (spectral–spatial) image of the whole pepper seed is shown in Fig. 8. The relatively sharp peak at the central region was used for 2D imaging.

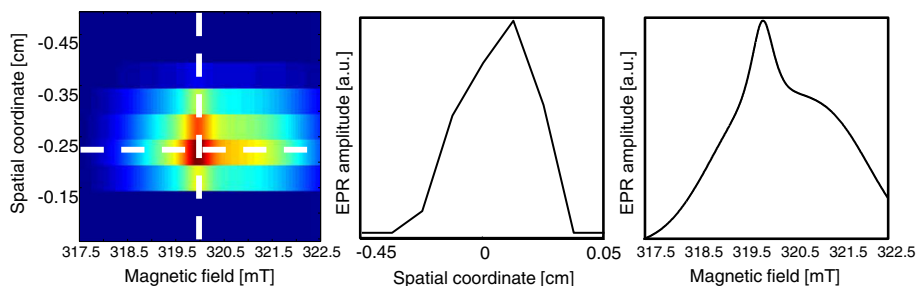


Fig. 8. 2D (spectral–spatial) images of the black pepper seed. The resolution is not good because of the strong background signal (Mn^{2+} related signals), which is truncated by the acquisition window.

We used iterative parametric reconstruction to overcome the broad background signals in poison filtered back-projection reconstructions. The spectral shape of the signals was estimated from a zero gradient spectra. The spatial distribution was the optimization parameter. In the left-hand panel of Fig. 8, the spatial coordinate of the Y-axis shows that the signals were within 2 mm in size. Images show signals from all areas because of the low image resolution and paramagnetic species distributed all over the surface area of the pepper.

For proper reconstruction of the images using filtered back-projection, complete support of an object in spatial and spectral domains was required. This was hard to achieve for the relatively sharp peak overlapping with a very broad signal observed in the pepper. The development of region of interest (ROI) imaging in the spectral domain can potentially be instrumental. ROI reconstruction of spatial images has been demonstrated previously [16]. The present EPR imaging may not resolve the inner core of the seed. To achieve a better resolution we may need to perform 2D or 3D imaging with higher applied magnetic field gradients.

Furthermore, the 9 GHz EPR imaging may provide noninvasive information regarding environmental damages, such as UV irradiation, radiation, and corruption and/or physical damages inside the materials. The location (region) of the paramagnetic (or free radicals induced) species can be used as a guide for further research on biochemistry or chemistry of paramagnetic species.

Conclusions

A noninvasive 9 GHz EPR imager and CW EPR were used to investigate paramagnetic species in the whole black pepper seeds. CW EPR measured a minimum of three distinguishable paramagnetic species. The EPR imaging was able to resolve samples spaced at ~ 2 mm. The EPR imager was also capable of generating 2D (spectral–spatial) imaging of black pepper seeds. The present results suggest that paramagnetic species were located on the surface of the pepper seed. The 9 GHz EPR imaging and CW EPR can be useful for detecting and identifying the location of paramagnetic species in foodstuffs and other small materials.

Acknowledgements

Part of this research was supported by Grant-in-Aid for Exploratory Research (24650247) and Grant-in-Aid for Scientific Research (B) (25282124) from Japan Society for the Promotion of Science (JSPS) (K.N.), and NIH Grants Numbers P41 EB002034 and R01 CA98575 (B.E.).

Appendix A. Supplementary material

Supplementary data associated with this article can be found, in the online version, at <http://dx.doi.org/10.1016/j.saa.2014.04.100>.

References

- [1] M. Ukai, Y. Shimoyama, *Appl. Magn. Reson.* 24 (2003) 1–11.
- [2] N.D. Yordanov, V. Gancheva, *Appl. Rad. Iso.* 52 (2000) 195–198.
- [3] R.W.A. Franco, L. Martin-Neto, M.S.A. Kato, G.R. Furlan, J.M.M. Walder, L.A. Colnago, *Int. J. Food Sci. Technol.* 39 (2004) 395–401.
- [4] M. Polovka, V. Brezová, A. Staškob, M. Mazúr, M. Suhaj, P. Šimko, *Rad. Phys. Chem.* 75 (2006) 309–321.
- [5] K. Nakagawa, Y. Ohba, B. Epel, H. Hirata, *J. Oleo Sci.* 61 (2012) 451–456.
- [6] M.M. Maltempo, S.S. Eaton, G.R. Eaton, *J. Magn. Reson.* 72 (1987) 449–455.
- [7] G.R. Eaton, S.S. Eaton, K. Ohno, CRC Press, FL, 1991.
- [8] B. Epel, H.J. Halpern, *Royal Soc. Chem.* 23 (2013) 180–208.
- [9] S. Subramanian, M.C. Krishna, *Magn. Reson Insights* 2 (2008) 43–74.
- [10] G.A. Rinard, R.W. Quine, S.S. Eaton, G.R. Eaton, *J. Magn. Reson.* 156 (2002) 113–121.
- [11] K. Nakagawa, *Cell. Mol. Biol.* 46 (2000) 1375–1381.
- [12] K.J. Liu, P. Gast, M. Moussavi, S.W. Norby, N. Vahidi, T. Walczak, M. Wu, H.M. Swartz, *Proc. Natl. Acad. Sci. USA* 90 (1993) 5438–5442.
- [13] K.H. Ahn, H.J. Halpern, *J. Magn. Reson.* 185 (2007) 152–158.
- [14] K. Nakagawa, *Free Rad. Res.* 48 (6) (2014) 679–683.
- [15] J.E. Wertz, J.R. Bolton, *Electron Spin Resonance*, Chapman and Hall Ltd., NY, 1986 (Chapter 11 and 12).
- [16] X. Pan, D. Xia, H. Halpern, *J. Magn. Reson.* 187 (2007) 66–77.